Geomechanics and Engineering, *Vol. 34, No. 3 (2023) 303-316*
https://doi.org/10.12989/gae.2023.34.3.303

Seismic deformation behaviors of the soft clay after freezing-thawing

Zhen-Dong Cui*, Meng-Hui Huang, Chen-Yu Hou and Li Yuan

State Key Laboratory of Intelligent Construction and Healthy Operation & Maintenance of Deep Underground Engineering, School of Mechanics and Civil Engineering, China University of Mining and Technology, Xuzhou, Jiangsu 221116, P. R. China

(*Received February 24, 2023, Revised June 15, 2023, Accepted June 29, 2023*)

Abstract. With the development and utilization of urban underground space, the artificial ground freezing technology has been widely used in the construction of underground engineering in soft soil areas. The mechanical properties of soft clay changed greatly after freezing and thawing, which affected the seismic performance of underground structures. In this paper, a series of triaxial tests were carried out to study the dynamic response of the freezing-thawing clay under the seismic load considering different dynamic stress amplitudes and different confining pressures. The reduction factor of dynamic shear stress was determined to correct the amplitude of the seismic load. The deformation development mode, the stress-strain relationship and the energy dissipation behavior of the soft clay under the seismic load were analyzed. An empirical model for predicting accumulative plastic strain was proposed and validated considering the loading times, the confining pressures and the dynamic stress amplitudes. The relevant research results can provide a theoretical reference to the seismic design of underground structures in soft clay areas.

Keywords: deformation mode; freezing-thawing; seismic load; soft clay

1. Introduction

Artificial ground freezing technology has been widely used in the construction of subway, tunnels and other large underground engineering (Jin *et al.* 2021, Zheng *et al.* 2021). In the coastal area, the soft clay layer is widely distributed and its water content is rich, which brings many problems and challenges to the construction of underground engineerings. After the artificial ground freezing, the frozen soil wall resulted from the saturated soft clay could be used as both a water retaining barrier and a structural support (Afshani and Akagi 2015, Zhou and Tang 2015b) during the construction to ensure the safe construction conditions and shorten the construction period. However, due to the existence of freezing-thawing cycles in the construction process, the soil structure changed a lot (Zhou and Tang 2015a), and the relevant properties also deteriorated. Historical earthquake damage showed that the seismic performance of underground structures in soft soil foundation was far less than expected, and the earthquake may cause more serious consequences (Iida *et al.* 1996, Wang *et al.* 2009, Murcia-Delso *et al.* 2020). Therefore, it is urgent to study the dynamic characteristics of soft clay after freezing-thawing under the seismic load.

After the freezing-thawing cycle, the properties and microstructures of soft clay would change, and exhibited more complex mechanical behaviors under the seismic load. The effects of freezing-thawing cycles on the characteristics of clay were studied (Yilmaz and Fidan 2018, Cheng *et al.* 2021). The freezing-thawing cycle played an important role for physical properties of soil (Ghazavi and Roustaei 2013).

In the process of freezing and thawing, the volume change caused by pore water icing up resulted in the change of pore characteristics and the rearrangement of soil particles. With the change of physical properties during the freezing-thawing process, the mechanical behaviors tended to be different at the same time, and a new dynamic balance was achieved within the soil mass (Yao *et al.* 2009). After the freezing-thawing cycle, the soil became looser and the void ratio increased (Wang *et al.* 2019), which led to greater strain under the loading (Kang and Lee 2015). Chamberlain and Gow (1979) observed that freezing-thawing cycles improved the permeability of clay. Later, the change mechanism of soil permeability was interpreted as the closure of micro cracks and the formation of large voids in the process of freezing-thawing (Tang and Yan 2014). The elastic modulus of clay decreased and the reduction degree was related to the temperature of the freezing-thawing process (Simonsen *et al.* 2002). Wang *et al*. (2007) found that the cohesion of the sample decreased and the internal friction angle increased after the freezing-thawing cycle. The physical and mechanical properties of soil samples tended to be a stable state with the critical number of freezing-thawing cycles (Zhou *et al.* 2018).

The mechanical behavior and deformation development of clay under dynamic load is a key problem for the design and construction of geotechnical engineering. On the one hand, the previous research mainly discussed the dynamic response of clay under the traffic load, less under the seismic load. The frequencies (Zhang and Cui 2018), vibration numbers and amplitudes of dynamic load (Ling *et al.* 2013) and test confining pressures (Yang *et al.* 2010) affected the change of soil properties. Under the dynamic loading, soft clay exhibited obvious nonlinear and hysteretic

*Corresponding author, Professor
E-mail: cuizhendong@cumt.edu.cn

ISSN: 2005-307X (Print), 2092-6219 (Online)

behavior (Ling *et al.* 2009). The stress-strain relationship of remolded ELO clay undergoing freezing-thawing process in undrained triaxial tests showed a strengthened behavior (Alkire and Morrison 1983). Guo *et al*. (2020) found that the accumulation of pore water pressure under undrained conditions contributed to the softening of clay, and the dynamic elastic modulus of clay decreased with the cyclic loading times increasing. Mansour (2018) and Cui *et al*. (2023) established relevant empirical formulas to predict the maximum dynamic shear modulus, damping ratio and other parameters of clay under the seismic load. On the other hand, it is difficult to describe the mechanical properties of clay under external loads due to the anisotropy and inhomogeneity of clay and the various effects of freezing-thawing process on structural parameters of clay. The mathematical models were concerned by many scholars to study the mechanical behavior of soil materials (Wang *et al.* 2021). Based on the disturbed state concept (DSC) and static triaxial test, Cui *et al.* (2014) proposed the constitutive model of thawed clay. Due to the strong non-linear characteristics of clay, there is a large deviation between the model and the experimental results when the strain is large. Puppala *et al.* (2009) proposed a permanent strain model with four parameters, and determined the contribution of confining pressure and deviatoric stress to the plastic strain by means of the multiple nonlinear regression analysis. Cui and Zhang (2015) analyzed the transformation between the Hardin-Drnevich model and the Martin-Davidenkov model, and conducted cyclic triaxial tests to verify the applicability of the two models to the dynamic backbone curve of the saturated soft clay. The high-cycle accumulation model (HCA) proposed by Niemunis *et al.* (2005) was improved and promoted by Wichtmann *et al.* (2010) and its empirical model being suitable for describing the accumulative plastic strain behavior of clay in cold regions was proved by Li *et al*. (2013), Lin *et al.* (2017) and Lei *et al*. (2019), respectively. The above related research can provide a reference for studying the dynamic characteristics of clay under the seismic load, but the further research should be conducted for the uncertainty of seismic load and the severity of seismic disaster.

In this paper, a series of triaxial tests were carried out to study the dynamic response of clay after freezing-thawing under the seismic load considering the dynamic stress amplitude and the confining pressure. The reduction factor of dynamic shear stress was determined to correct the seismic load. The deformation development mode, the stress-strain relationship and the energy dissipation behavior of soft clay under the seismic load were analyzed and discussed. The empirical model considering the loading times, the confining pressures and the dynamic stress amplitudes was proposed and validated.

2. Experiment preparation

2.1 The reduction factor of dynamic shear stress

The seismic wave is random and uneven in the process of propagation and the shear stress is also irregular. According to the anti-liquefaction shear stress method proposed by Seed and Idriss, called Seed's Method, the indoor dynamic triaxial test can be carried out by cyclic loading with the constant amplitude of dynamic shear stress, so as to simulate the effect of seismic shear stress. Seed suggested that the shear stress $\overline{\tau}_{\mathrm{e}}$ under uniform amplitude action should be 0.65 times of the maximum shear stress $\tau_{\max}$ of the actual earthquake.

$$\overline{\tau}_{\mathrm{e}} = 0.65\tau_{\max} \tag{1}$$

The soil between the point at depth h and the ground surface was assumed to be a rigid body for calculating the maximum seismic shear stress. The inertia force in the horizontal direction and the shear force in the horizontal plane for the rigid soil at depth h balance each other, so the maximum seismic shear stress of soil layer at depth h can be obtained.

$$\left(\tau_{\max}\right)_{\text{rigid-body}} = \sigma_{\mathrm{v}} \frac{a_{\max}}{g} \tag{2}$$

where σ_{v} is the total normal stress of soil layer at depth h; g is the acceleration of gravity; $a_{\max}$ is the peak ground acceleration.

In the process of actual ground motion propagation, due to the attenuation effect of the soil layer, the shear stress of the soil is smaller than that of the rigid body, that is, the actual seismic shear stress $(\tau_{\max})_{\text{real}}$ is smaller than that calculated by Formula (2). Therefore, the reduction factor of dynamic shear stress γ_{d} was introduced to reduce the dynamic shear stress according to the rigid soil, as shown in Formula (3).

$$\left(\tau_{\max}\right)_{\text{real}} = \gamma_{\mathrm{d}} \left(\tau_{\max}\right)_{\text{rigid-body}} \tag{3}$$

The expression of the reduction factor of dynamic shear stress was defined by Formula (4).

$$\gamma_{\mathrm{d}} = \frac{\left(\tau_{\max}\right)_{\text{real}}}{\left(\tau_{\max}\right)_{\text{rigid-body}}} \tag{4}$$

Based on Seed's Method, the reduction factor of dynamic shear stress depended on the density and depth of the soil. For shallow soil buried at a depth of about 10m, the impact of soil density on the reduction factor of dynamic shear stress was relatively small. Hence, the influence of soil density was ignored to simplify the calculation. The variations of the reduction factor of dynamic shear stress with depth was shown in Formula (5) from Seed's Method.

$$\begin{cases} \gamma_{\mathrm{d}} = 1.0 - 0.00765h & \left(h \le 9.15\right) \\ \gamma_{\mathrm{d}} = 1.174 - 0.0267h & \left(9.15 < h \le 23\right) \end{cases} \tag{5}$$

The reduction factor of dynamic shear stress from Seed's Method was widely used in the earthquake engineering. However, there were some limitations for Seed's Method. Firstly, few models were used for site seismic response analysis, which did not cover the site conditions encountered in the actual project. Secondly, the

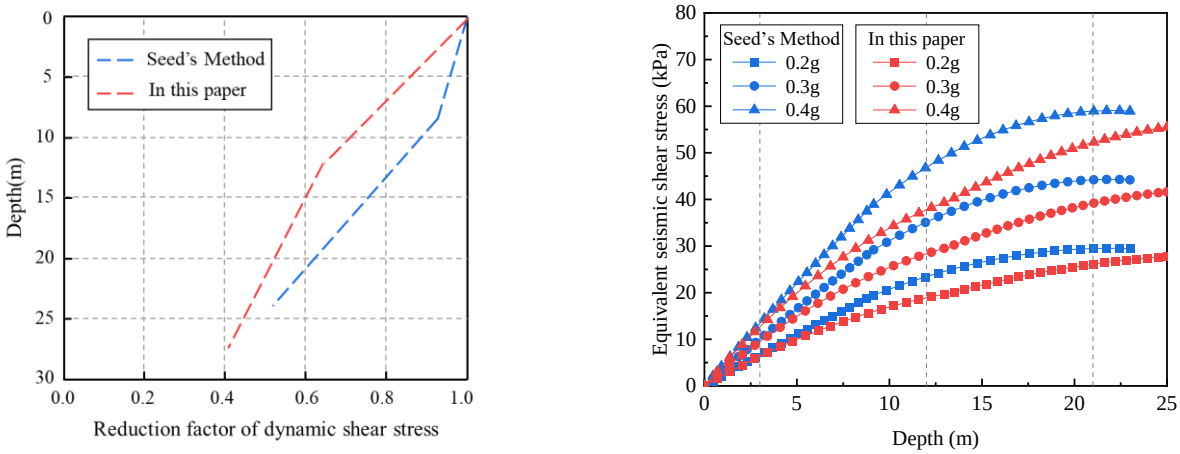

(a) reduction factor of dynamic shear stress (b) equivalent seismic shear stress

Fig. 1 Comparison between the method in this paper and Seed's Method for: (a) reduction factor of dynamic shear stress and (b) equivalent seismic shear stress

Table 1 Basic physical parameters of soil sample

Soil property	Water content (%)	Density (g/cm^3)	Void ratio	Plasticity index	Modulus of compressibility (MPa)
U	47.8	1.76	1.013	15.4	4.60
F	47.1	1.77	1.060	17.2	3.88

soil layer in the site models was too ideal and had significant differences from that of the actual site conditions. Thirdly, Seed's Method was mainly applicable to assessment of liquefaction susceptibility for sand and sand sites, and it was not determined whether it was suitable for clay. In response to the shortcomings of the Seed's Method, seismic response analysis for undisturbed clay site and freezing-thawing clay site was conducted by DEEPSOIL. The maximum shear stress of the soil layer was obtained under the different peak ground accelerations. Then, the corresponding reduction factor of dynamic shear stress for undisturbed clay site and freezing-thawing clay site was calculated by combining Formulas (2) and (4), as shown in Formula (6). The reduction factor of dynamic shear stress obtained in this paper was compared with Seed's Method, as shown in Fig. 1(a). It can be seen that the reduction factor of dynamic shear stress obtained in this paper was smaller than Seed's Method within a finite depth.

The attenuation effect of clay sites or freezing-thawing clay sites on seismic motion was greater than that of sand sites. For the depth from surface to 13.5 m, the attenuation rate of seismic motion in clay sites is relatively fast.

$$\begin{cases} \gamma_d = 0.99546 - 0.02592h & (h \le 13.5) \\ \gamma_d = 0.84370 - 0.01445h & (13.5 < h \le 30) \end{cases} \quad (6)$$

The uniform equivalent seismic shear stress for freezing-thawing clay soil at different depths was obtained by substituting Formula (6) into Formulas (1-3). According to the measured seismic records from PEER and COSMOS (Singh *et al.* 2023), 0.2 *g*, 0.3 *g* and 0.4 *g* were taken as the peak ground acceleration during the earthquake. If the unit weight of soil is 17.7kN/m^3, the variations of uniform equivalent seismic shear stress with depth from this paper and Seed's Method were shown in Fig. 1(b), respectively.

From the figure, the change of equivalent seismic shear stress with depth proposed in this paper is more uniform. Within the finite depth range, the equivalent seismic shear stress from this paper is less than that from Seed's Method. As the peak ground acceleration increases, the maximum value of the difference in equivalent seismic shear stress obtained by the two methods increases. The reduction factor of dynamic shear stress from Seed's Method will overestimate the uniform equivalent seismic shear stress of freezing-thawing clay site.

2.2 Experimental process

The soil sample was taken from the muddy clay of Layer No.4 in Shanghai, and the buried depth was about 15 m. In order to reduce disturbance, the sampling process should be careful. After taking out, the soil sample was tightly wrapped by iron bucket and plastic film to prevent moisture loss. The basic physical parameters of the soil sample are summarized in Table 1.

As the low temperature near zero may lead to incomplete freezing or even non-freezing, the soil sample was frozen at -10℃ for 48 hours and melted at 20℃ in order to ensure that the soil sample is fully and completely frozen. In the process of freezing and thawing, the soil sample was always wrapped by plastic film to avoid water loss (evaporation). Dynamic triaxial test was conducted by using DYNTTS equipment produced by GDS company. The maximum axial force of the testing system is 5 kN, the maximum loading frequency is 5 Hz, and the maximum confining pressure is 2 MPa. The dynamic wave for

Table 2 Equivalent seismic shear stress

	0.2 *g*	0.3 *g*	0.4 *g*
3 m	6.2 kPa	9.3 kPa	12.4 kPa
12 m	18.6 kPa	27.9 kPa	37.2 kPa
21 m	25.7 kPa	38.5 kPa	51.3 kPa

Table 3 Test scheme

Soil number	Soil property	Effective confining pressure $\sigma_3^{'}$ (kPa)	Frequency f (Hz)	Dynamic stress amplitude σ_d (kPa)	Number of cyclic loading N
D1	F(-10℃)	30.9	1	6.2	7200
D2	F(-10℃)	30.9	1	9.3	7200
D3	F(-10℃)	30.9	1	12.4	7200
D4	F(-10℃)	123.6	1	18.6	7200
D5	F(-10℃)	123.6	1	27.9	7200
D6	F(-10℃)	123.6	1	37.2	7200
D7	F(-10℃)	216.3	1	25.7	7200
D8	F(-10℃)	216.3	1	38.5	7200
D9	F(-10℃)	216.3	1	51.3	7200

DYNTTS can be sine wave, square wave or triangular wave. The sine wave was selected in this test. Based on Formula (7), the effective confining pressure during consolidation was taken as 30.9 kPa, 123.6 kPa and 216.3 kPa according to the simulated depth, respectively.

$$\sigma_3^{'} = K_0\sigma_1^{'} = K_0(\gamma h - \psi\gamma_w h) \quad (7)$$

where $\sigma_1^{'}$ and $\sigma_3^{'}$ is the effective axial pressure and effective confining pressure during consolidation, respectively; K_0 is the coefficient of static earth pressure; γ and γ_w are the unit weight of soil and water, respectively; h is the depth of soil sample; ψ is the reduction factor of lateral water pressure, being 0.7 for clay (Cui *et al.* 2019).

According to the equivalent seismic shear stress of freezing-thawing clay site obtained in Section 2.1, the equivalent seismic shear stress under different depths and peak ground accelerations is obtained, as shown in Table 2, corresponding to the location of the dotted line in Fig. 1(b).

By analyzing the spectrum characteristics of the measured seismic time history curve, it is concluded that the seismic predominant frequency is generally in the range of 1.4~7.25 Hz, and its fundamental frequency is generally about 1 Hz. The loading frequency was set as 1 Hz in this test. During the test, the soil sample was cut into cylinders with a height of 100 mm and a diameter of 50 mm. In order to ensure good drainage conditions during the consolidation, the strip filter paper was uniformly attached to the surface of the soil sample. The sample was saturated by back pressure until the B value reached 0.95, and then the sample was consolidated under equipressure.

Considering the low permeability of clay, stress controlled cyclic triaxial tests were carried out under consolidated undrained conditions. The test scheme is shown in Table 3.

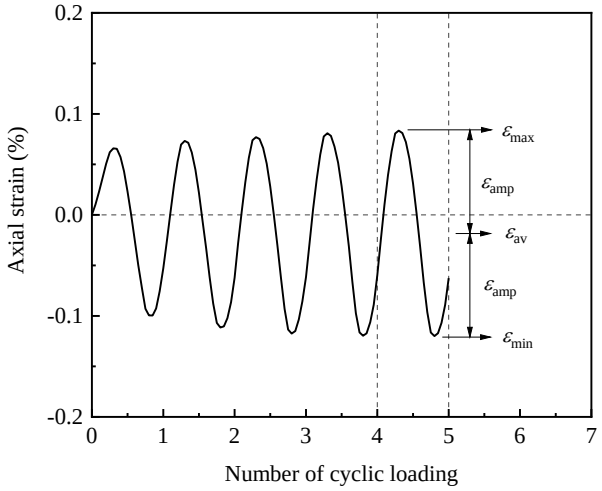

Fig. 2 Quantitative strain diagram

3. Experimental results and discussion

3.1 Axial strain

As shown in Fig. 2, ε_{max} and ε_{min} are defined as the maximum axial strain and the minimum axial strain in each cycle, respectively; ε_{amp} is the cyclic strain amplitude, which is $(\varepsilon_{max}-\varepsilon_{min})/2$; ε_{av} is the average strain, which is $(\varepsilon_{max}+\varepsilon_{min})/2$. Fig. 3 illustrates the variation of the axial strain with the cyclic loading time under the different confining pressures and peak ground accelerations. With the increase of number of cyclic loading, ε_{amp} gradually increases and tends to be stable. At the same time, the greater the surface peak acceleration, the greater the ε_{amp}, and the faster the increase speed. It can be understood that the greater the peak ground acceleration, the more energy transmitted by the cyclic load to the soil sample, and the greater the plastic deformation of the soil sample. With the increase of the number of cycles, the plastic deformation of soil samples continues to accumulate.

When the confining pressure is small, it can be seen from the Fig. 3(a) that ε_{max} decreases and ε_{min} increases. In other words, the axial strain of soil sample continues to develop to tensile strain under the cyclic loading, which means that ε_{av} continues to develop in a negative direction. When the confining pressure increases to be 123.6 kPa, both ε_{max} and ε_{min} gradually increase, the development of axial strain is almost symmetrical, and ε_{av} is approximately zero. However, it should be noted that the development speed of ε_{max} to the positive strain is slightly less than that of ε_{min} to the negative strain, and ε_{av} shows a trend of negative strain. When the confining pressure reaches 216.3 kPa, ε_{av} first develops in the negative direction at the initial stage of loading, and then starts to develop in the positive direction after several cycles. In addition, the larger the

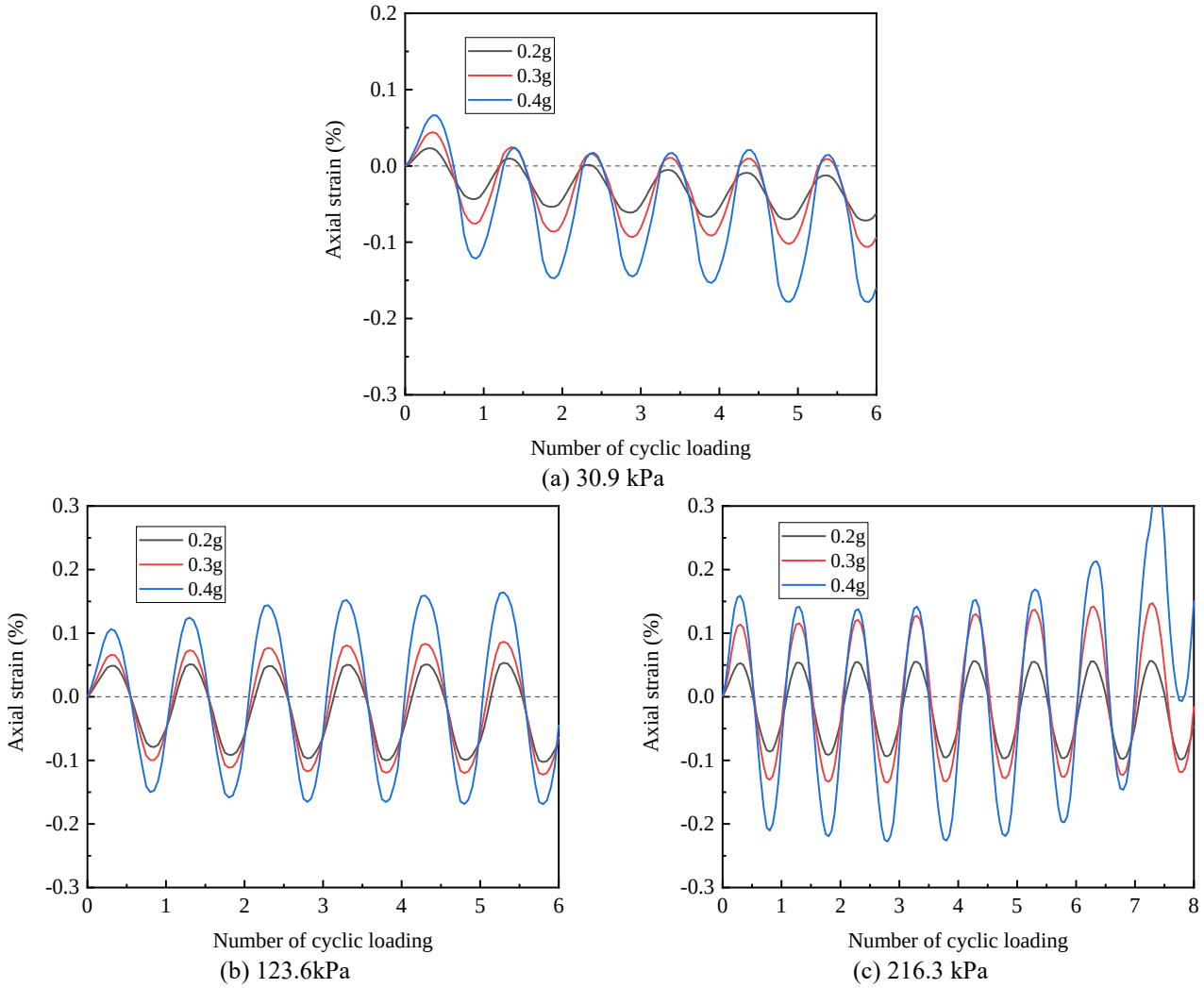

Fig. 3 Variations of axial strain with number of cyclic loading for the freezing-thawing clay at different confining pressures: (a) 30.9 kPa, (b) 123.6 kPa and (c) 216.3 kPa

peak ground acceleration is, the faster the soil sample develops to positive strain. With the peak ground acceleration being 0.4g, the soil sample develops to positive strain from the 6th number of cyclic loading. With the peak ground acceleration being 0.3 g, 26 loading cycles are needed for the positive strain. When the peak ground acceleration is 0.2 g, the sample does not change significantly.

3.2 Accumulative plastic strain

3.2.1 The development of accumulative plastic strain

Fig. 4 illustrates the variations of the accumulative plastic strain with number of cyclic loading of freezing-thawing clay under the different confining pressures and peak ground accelerations. The confining pressure has an important effect on the accumulative plastic strain of the freezing-thawing clay. With the confining pressure increasing, the development of cumulative plastic strain curve of freezing-thawing clay shows obvious difference.

When the confining pressure is small, it can be seen from Fig. 4(a) that the soil sample shows the tensile deformation under the cyclic load, and the tensile strain continues to develop with the number of cyclic loading increasing. The soil sample is subjected to cyclic load in the equipressure condition and the deviator stress is less than zero for half of each loading cycle. In other words, when the axial pressure is less than the confining pressure, the soil sample is extruded and elongated.

When the effective confining pressure increases from 30.9 kPa to 123.6 kPa, the freezing-thawing clay changes from the tensile strain to the compressive strain under the cyclic loading. The transformation of deformation mode can be explained from two aspects. On the one hand, with the confining pressure increasing, the normal stress on the shear plane of soil sample increases significantly, which directly leads to the enhancement of anti-sliding friction. On the other hand, under the large consolidation pressure, the consolidation and compaction process of soil samples makes the soil particles closer and improves the internal embedding force among soil particles. It can be inferred that soil particles slip and rearrange during the consolidation and compaction, forming a more stable soil skeleton, and the anti-deformation ability of soil under the cyclic loading is

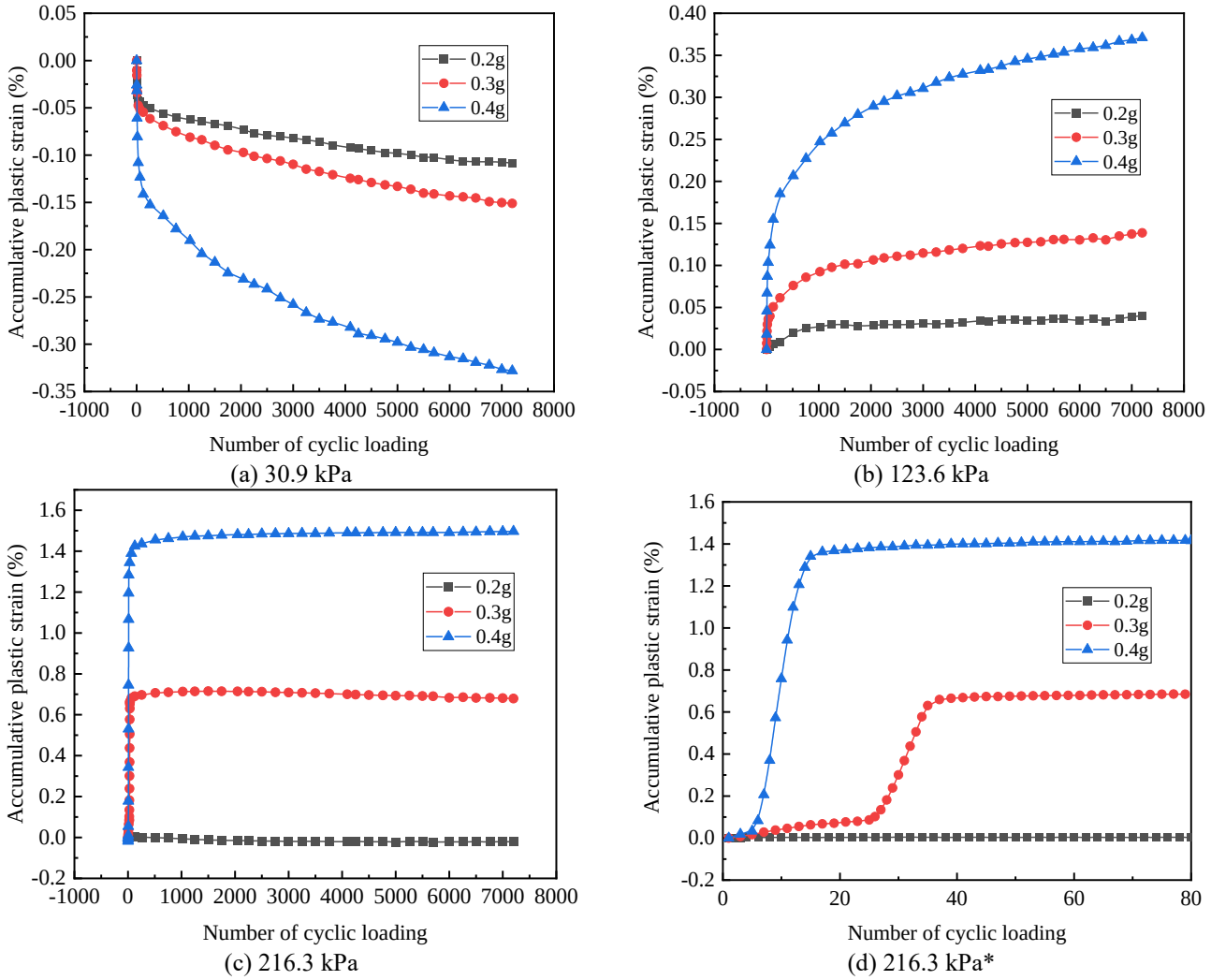

Fig. 4 Variations of accumulative plastic strain with number of cyclic loading for the freezing-thawing clay at different confining pressures: (a) 30.9kPa, (b) 123.6kPa, (c) 216.3kPa and (d) 216.3kPa*

enhanced. Compared with the smaller confining pressure, the deviator stress is all greater than zero for each loading cycle under the larger confining pressure, which dominates the deformation of the soil sample. It can be inferred that there is a critical effective confining pressure between 30.9 kPa and 123.6 kPa. The soil sample subjected to the greater than the critical effective confining pressure exhibits the compressive strain under the cyclic loading. The soil sample subjected to the less than the critical effective confining pressure shows the tensile strain under the cyclic loading. In addition, it can be seen from Fig. 4(b) that with the number of cyclic loading increasing, the development of the accumulative plastic strain of the soil sample can be divided into two stages: the rapid growth stage and the slow growth stage. The consolidation of the soil sample is completed in the equipressure condition and the soil sample receives a large stress amplitude in the axial direction with the cyclic loading. The soil sample cannot respond quickly, resulting in a large initial strain.

When the confining pressure reaches 216.3 kPa, as shown in Figs. 4(c) and 4(d), the plastic strain of the soil sample only accumulates at the initial stage of loading and reaches a stable state after several cycles. Compared with the confining pressure, the effect of the cyclic loading on the accumulative plastic strain of soil sample can be ignored. This means that after the soil is consolidated under the large consolidation pressure, its strength and the ability to resist deformation under the cyclic loading is stronger.

The peak ground acceleration has an important effect on the accumulative plastic strain of the freezing-thawing soil. The accumulative plastic strain of soil sample increases with the peak ground acceleration increasing, whether the tensile strain or the compressive strain. It is worth noting that the tangent modulus of the curve decreases with the number of cyclic loading increasing until it reaches stability. Then the soil sample is continuously deformed.

The maximum deformation and initial tangent modulus increase significantly with the increase of the peak ground acceleration. It should be noted that the accumulative plastic strain of the soil sample with the larger confining pressure suddenly changes after less cycles. The greater the peak ground acceleration, the less the number of cyclic loading required for the sudden change, and the greater the sudden change.

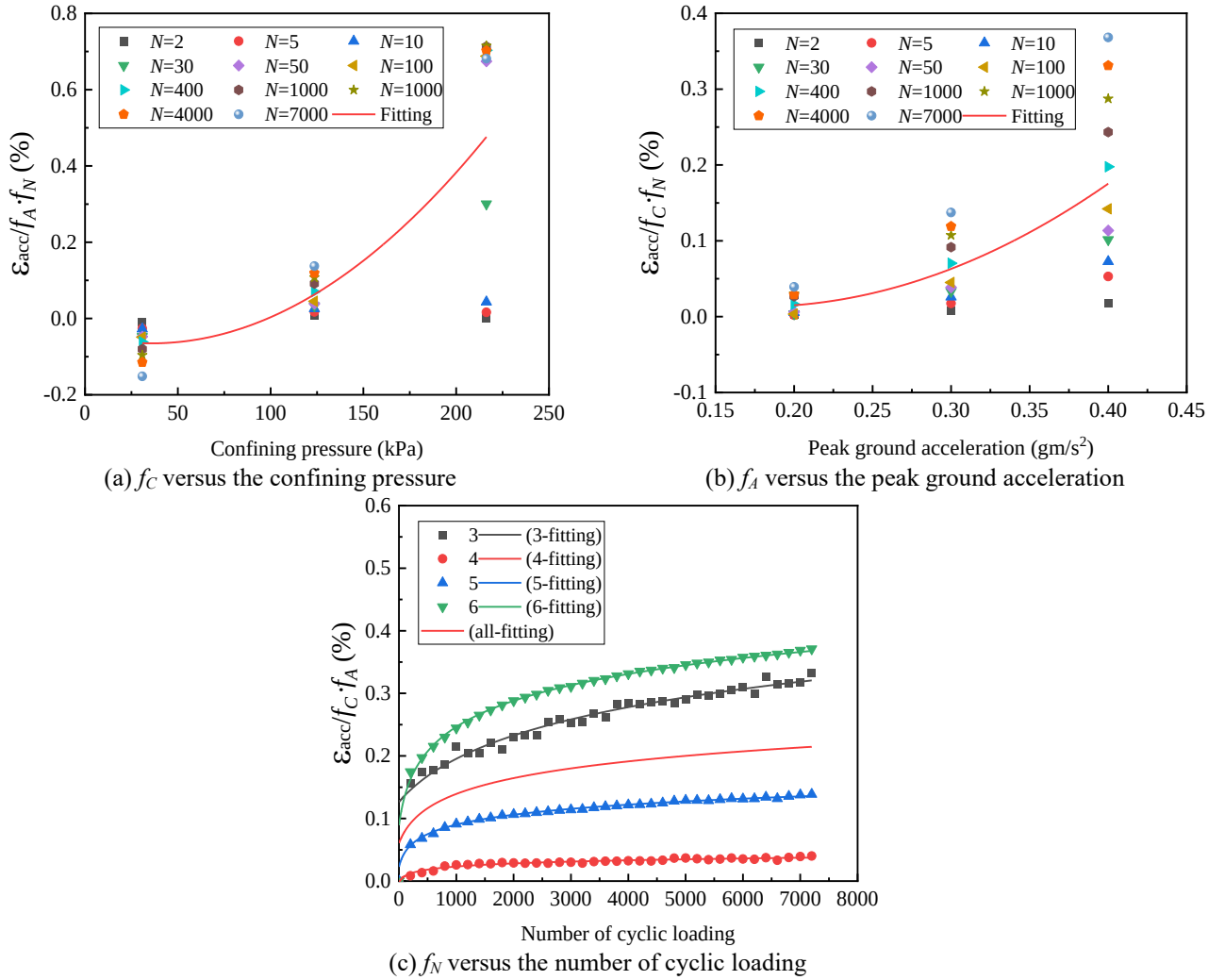

(a) f_C versus the confining pressure

(b) f_A versus the peak ground acceleration

(c) f_N versus the number of cyclic loading

Fig. 5 Contribution of correction functions for three influence factors to accumulative plastic strain

3.2.2 The model of accumulative plastic strain

The above analysis shows that the effects of confining pressure, dynamic stress amplitude and loading times on the accumulative plastic strain development of freezing-thawing clay are complex and diverse. The research model in this paper aims to determine the contribution of each influencing factor to the development of accumulative plastic strain. An empirical model derived from the high-cycle accumulation model (Niemunis *et al.* 2005) was developed by Wichtmann *et al*. (2010) for sand. And then it was proved by Li *et al.* (2013), Lin *et al*. (2017), Lei *et al.* (2019) that it is appropriate to describe the accumulative plastic strain behavior of clay in cold regions. In addition, the practicality and applicability of the empirical model have also been validated. Therefore, based on the existing research, an empirical model for predicting accumulative plastic strain of freezing-thawing clay is proposed, as shown in Formula (8).

$$\varepsilon_{\mathrm{acc}}(N) = f_C \cdot f_A \cdot f_N \tag{8}$$

where f_C is the correction function of confining pressure, reflecting the contribution of confining pressure to accumulative plastic strain; f_A is the correction function of seismic peak acceleration, reflecting the contribution of dynamic stress amplitude to accumulative plastic strain; f_N is the correction function of loading times, reflecting the contribution of loading times to accumulative plastic strain.

The relationship between normalized accumulative plastic strain and confining pressure is shown in Fig. 5(a). The quadratic function is selected to fit their relationship, which is described as Formula (9).

$$f_C = A_1 + A_2 \cdot \sigma_3 + A_3 \cdot \sigma_3^2 \tag{9}$$

where σ_3 is the confining pressure; A_1, A_2 and A_3 are the material constants.

The relationship between normalized accumulative plastic strain and peak ground acceleration is shown in Fig. 5(b). The quadratic function is selected to fit their relationship, which is described as Formula (10).

$$f_A = B_1 + B_2 \cdot a + B_3 \cdot a^2 \tag{10}$$

where a is the peak ground acceleration; B_1, B_2 and B_3 are the material constants.

The relationship between the normalized accumulative plastic strain and the number of cyclic loading is shown in

Table 4 Model parameters

Discussed factors	Modification functions	Material constants
Confining pressure	$f_C = A_1 + A_2 \cdot \sigma_3 + A_3 \cdot \sigma_3^2$	$A_1 = -0.04388$ $A_2 = -0.00119$ $A_3 = 1.66086 \times 10^{-5}$
Peak ground acceleration	$f_A = B_1 + B_2 \cdot a + B_3 \cdot a^2$	$B_1 = 0.11193$ $B_2 = -1.62764$ $B_3 = 1.76850$
Number of cyclic loading	$f_N = C_1 - C_2 \cdot \ln(N + C_3)$	$C_1 = -0.15016$ $C_2 = -0.04096$ $C_3 = 170.81021$

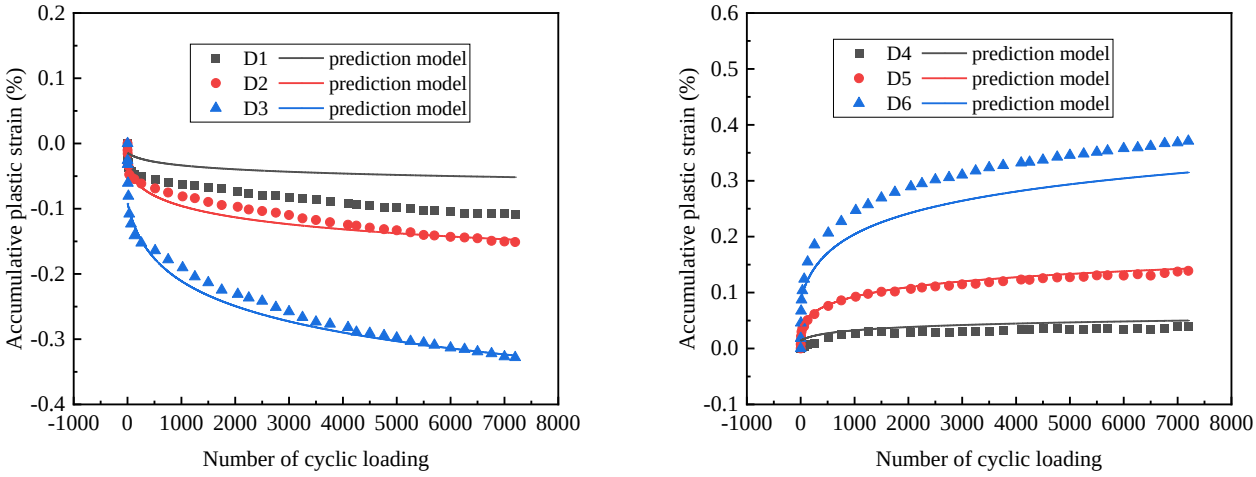

(a) 30.9 kPa (b) 123.6 kPa

Fig. 6 Comparison between the proposed model data and experimental data: (a) 30.9 kPa and (b) 123.6 kPa

Fig. 5(c). The logarithmic function is selected to fit their relationship, which is described as Formula (11).

$$f_N = C_1 - C_2 \cdot \ln(N + C_3) \tag{11}$$

where N is the number of cyclic loading; C_1, C_2 and C_3 are the material constants. The expression of each influencing factor and the values of the fitting material constants are summarized in Table 4.

In order to validate the prediction model proposed in this paper, the accumulative plastic strain respectively obtained from experimental measurements and model calculations are compared, and the consistency between the two values is shown in Fig. 6. When the confining pressure is small, the accumulative plastic strain prediction values obtained by Formula (8) gradually increase with the peak ground acceleration increasing; When the confining pressure is large, the predicted values decrease gradually with the peak ground acceleration increasing. Among the six groups used to verify the prediction model, except Group D1 and Group D6, the other four groups have a high degree of coincidence with the experimental data, and the predicted values are slightly larger than the experimental values, which is relatively safe. By analyzing the test conditions of Group D1 and Group D6, it is found that the prediction model has some errors and tends to be dangerous under small confining pressure and small acceleration or large confining pressure and large acceleration. It is expected to pay more attention in practical application. Although some predicted values fluctuate slightly, the most of predicted values are located around the experimental data closely under different confining pressures, peak ground accelerations and loading times. It can be summarized that the prediction model proposed in this paper is suitable for describing the accumulative plastic strain behavior of freezing-thawing clay under the cyclic loading.

3.3 Hysteresis curve

Under the cyclic loading, the excess pore water pressure generated and accumulated in the saturated soft clay, which leads to the reduction of the effective stress of the soil and the degradation of the stiffness or strain softening of the soft clay. This phenomenon is called stiffness degradation or strain softening. In the dynamic triaxial test, the stiffness of the soil can be expressed by the secant modulus E of the hysteretic curve, as shown in Fig. 7 and Formula (12). The greater the secant modulus, the greater the stiffness of the soil. Under the cyclic loading, the dynamic stress-strain relationship of soil forms a series of unclosed but continuous hysteretic cycles with the increase of time. With the number of cyclic loading increasing, the strain gradually develops, and the hysteretic cycle gradually moves to the right. The starting point and end point of the hysteretic curve do not coincide, and the change of location indicates that the soil has produced plastic strain and gradually accumulated. Under the cyclic loading, the stiffness degradation of the saturated soft clay occurs due to its nonlinearity, hysteresis and deformation accumulation. The hysteresis curve in Fig. 8 shows the stiffness degradation of soft clay with the gradual increase of the number of cyclic loading.

$$E = \frac{\sigma_{\max} - \sigma_{\min}}{\varepsilon_{\max} - \varepsilon_{\min}} \tag{12}$$

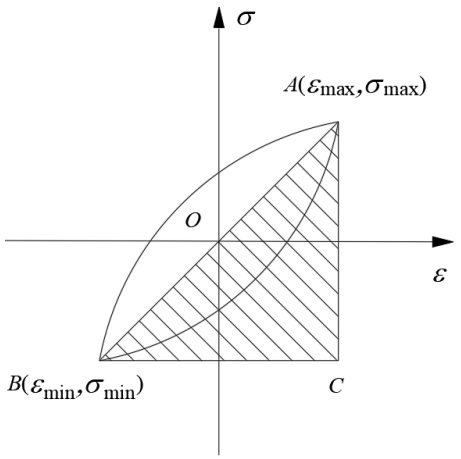

Fig. 7 Ideal hysteresis curve

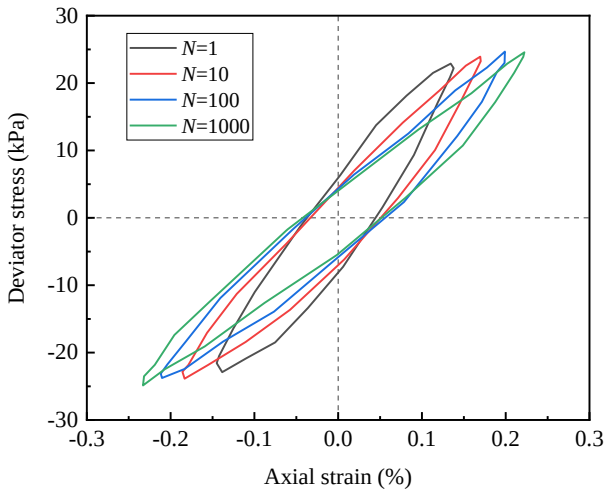

Fig. 8 Hysteresis curve under different loading times

3.3.1 Secant modulus

As shown in Fig. 7, the secant modulus of soil under the dynamic loading, that is, the stiffness of soil, is defined as the linear slope between the top and bottom points of a single hysteretic curve. Fig. 9 shows the variations of secant modulus of hysteresis curve with the number of cyclic loading of the freezing-thawing clay at different confining pressures. It can be seen from Fig. 9 that the change of secant modulus is very complex. On the whole, the change of secant modulus can be divided into two states, the rapid change stage and the stable fluctuation state. The secant modulus changes rapidly within 50 times of loading. The development of secant modulus shows different characteristics under different confining pressures. When the confining pressure is small, as shown in Fig. 9(a), the secant modulus generally decreases, and the stiffness of the soil weakens. It can be seen from Fig. 9(b) that when the confining pressure gradually increases, the change of secant modulus in the declining stage is more obvious than that when the confining pressure is small. On the whole, the soil still shows the trend of stiffness degradation. Under the cyclic loading, the structure of freezing-thawing soil changes and produces the compression deformation to squeeze the expanded pore volume in the process of freezing-thawing. Therefore, the secant modulus of soil decreases, the deformation accumulates and the stiffness weakens gradually. When the confining pressure reaches 216.3 kPa, it can be seen from Fig. 9(c) that the secant modulus first decreases and then increases under the cyclic loading. At the initial stage of loading, the secant modulus decays to a great extent, and the maximum value of reduction reaches 30%. In the subsequent loading, the secant modulus increases gradually, which may be related to the large stress amplitude of the soil sample at the initial loading stage and the large deformation of the soil sample. After that, the soil sample is continuously compressed under the cyclic loading, and the secant modulus gradually increases and finally fluctuates in a stable range. The stiffness of soil recovered after the degradation, which may be caused by the change of soil structures, the rearrangement of soil particles, or the phenomenon of shear expansion or shear shrinkage.

In addition, it can be seen from Fig. 9 that under the same confining pressure, the different peak ground accelerations also have a profound impact on the secant modulus. From Fig. 9(a), the greater the peak ground accelerations, the lower the secant modulus of the hysteresis curve, and the more the stiffness of the soil degenerates. This is mainly because the energy transmitted by the cyclic loading is different. Under the larger dynamic stress amplitude, the more energy the cyclic loading transfers to the soil, the greater the soil deformation, and the more obvious the stiffness degradation. When the confining pressure increases, from Figs. 9(b) and 9(c), the change of secant modulus caused by different peak ground accelerations is also different from that caused by small confining pressure. After 50 cycles of cyclic loading, the secant modulus corresponding to 0.3 g peak ground acceleration is the largest, and the secant modulus corresponding to 0.4 g is the smallest. With the increase of the peak ground acceleration, the secant modulus increases firstly and then decreases. On the one hand, the calculation of dynamic stress amplitude is related to the depth, and the amplitude of dynamic stress changes with the confining pressure. Therefore, there may be a coupling effect between the confining pressure and the amplitude of dynamic stress on test results. On the other hand, soil is a typical inhomogeneous and anisotropic material, and the influence of the differences between soil samples on the test results cannot be ignored.

3.3.2 Energy dissipation

Soft clay is a complex viscoelastic plastic medium. From the dynamic stress-strain hysteresis curve, it can be seen that the loading and unloading paths are not completely coincident like elastic media, instead, form an unclosed hysteresis cycle, which indicates that there are differences in energy changes between the loading and unloading processes. The work done by the exciting force on the sample during the loading process is mainly transformed into the internal energy of the sample, including the strain energy of the sample and the increase of pore water pressure. The relationship between the energy of work done by the external load of the sample and the

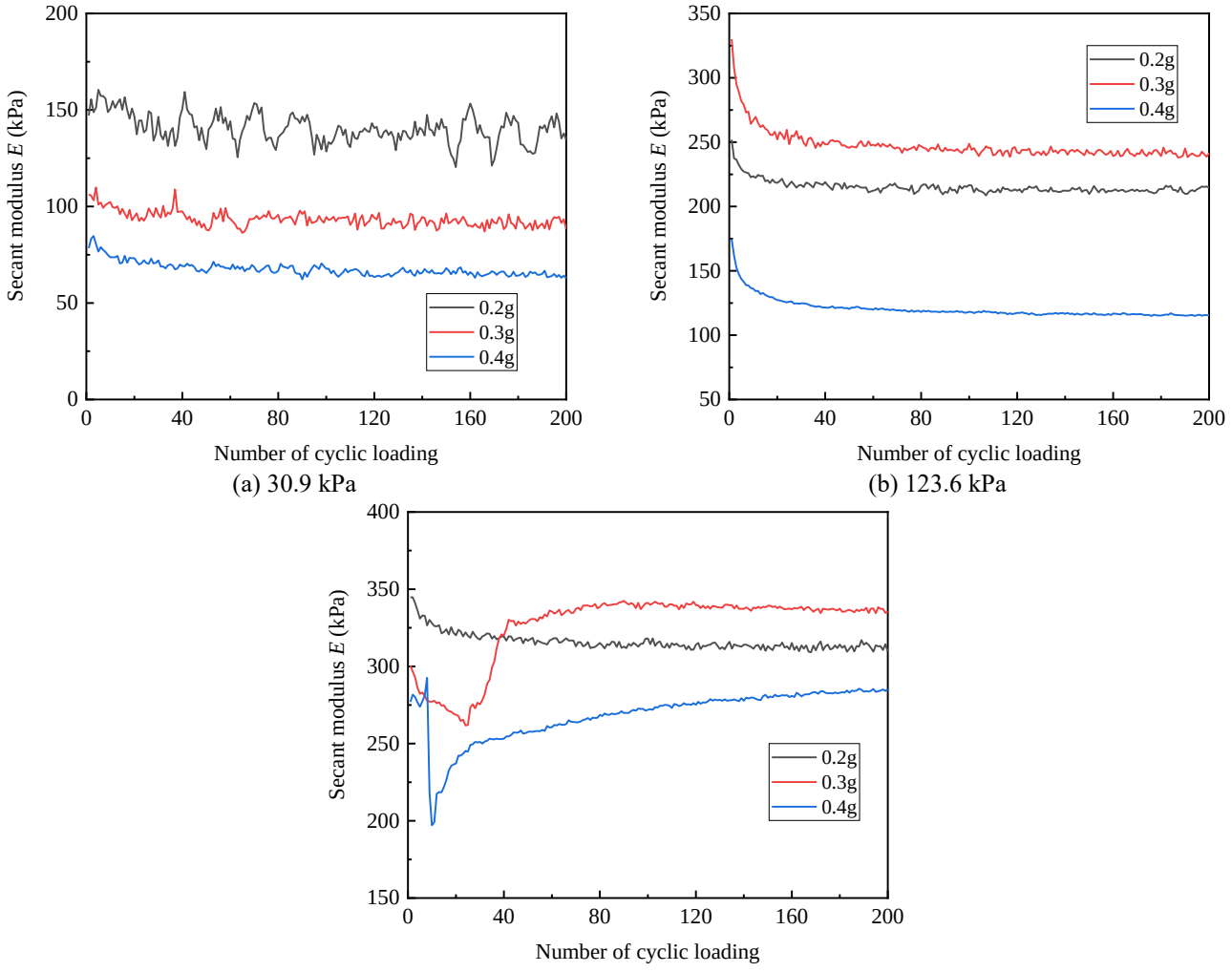

Fig. 9 Variations of secant modulus of hysteresis curve with the number of cyclic loading for the freezing-thawing clay at different confining pressures: (a) 30.9 kPa, (b) 123.6 kPa and (c) 216.3 kPa

internal energy of the sample is changeable. In the unloading process, some of the stored internal energy is released mainly in the form of elastic strain recovery and excess pore water pressure dissipation. The remaining energy is the damping dissipation energy of the soil.

Fig. 10 shows the variations of the area of the hysteresis loop of the freezing-thawing soil under the different confining pressures. The area of each hysteresis loop fluctuates unevenly up and down. The area of the hysteresis loop for most samples first increases briefly and then reaches a stable state with the number of cyclic loading increasing, that is, the energy dissipation becomes more and more stable. Under the different confining pressures, the area of hysteresis loop exhibits different characteristics. When the confining pressure is small, the area of the hysteresis loop of the freezing-thawing soil under the cyclic loading increases continuously and reaches a steady fluctuation state. When the confining pressure is large, the area of hysteresis loop of soil sample under the cyclic loading decays to varying degrees, especially when the confining pressure reaches 213.6 kPa. The main reason is that after freezing and thawing, the pore volume of the sample increases. After consolidation, the pore volume decreases. Under the cyclic loading, the pore volume of the soil further decreases, resulting in the gradual hardening of the soil and the smaller and smaller increment of plastic deformation. With the number of cyclic loading increasing, the area enclosed by hysteretic curve is gradually reduced, so the energy dissipation is less and less. In addition, in most cases, the greater the dynamic stress amplitude, the more energy transferred to the soil by the cyclic loading, the greater the energy dissipation, and the greater strain and pore water pressure of the soil sample.

3.3.3 Damping ratio

Damping represents the energy consumption of soil under cyclic load. The damping ratio, that is, the ratio of the actual damping coefficient to the critical damping coefficient, can be measured by the area of the stress-strain hysteresis curve during the loading and unloading, as shown in Fig. 7 and Formula (13).

$$\lambda = \frac{1}{4\pi}\frac{\Delta W}{W} \tag{13}$$

where ΔW is the area of single hysteresis loop; W is the total energy during the loading.

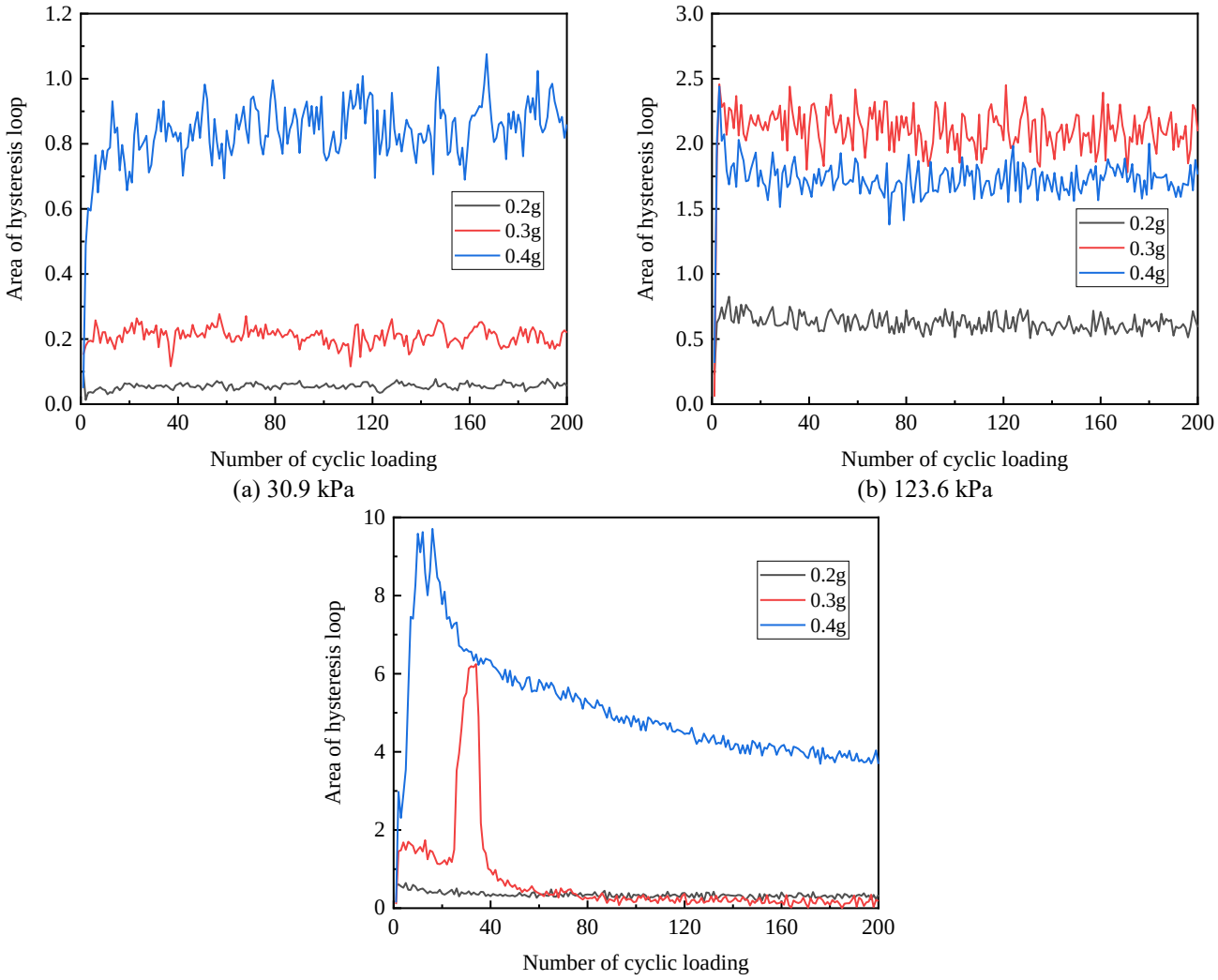

Fig. 10 Variations of area of hysteresis loop with the number of cyclic loading for the freezing-thawing clay at different confining pressures: (a) 30.9 kPa, (b) 123.6 kPa and (c) 216.3 kPa

Fig. 11 shows the variations of the damping ratio with the number of cyclic loading for the freezing-thawing clay under the cyclic loading at different confining pressures. The damping ratio corresponding to the hysteresis loop of the soil sample in each cycle fluctuates unevenly up and down with the increase of loading times, but the overall trend is gradually decreasing. The fluctuation of damping ratio with loading times can be explained as that the soil sample is saturated soft clay and belongs to low permeability soil. Under the cyclic loading, the excess pore water pressure rises rapidly, but the dissipation process is very long. This is also related to the undrained test conditions. Then, when the work done by the instrument on the soil is transformed into the strain energy and the excess pore water pressure, the instability is more likely to occur. Especially in this test, the fluctuation of excess pore water pressure is also obvious.

It can be seen from Fig. 11(a) that when the confining pressure is small, the damping ratio of the soil sample first increases and then reaches a stable state. When the confining pressure increases, from Figs. 11(b) and 11(c), the damping ratio of the soil sample first increases and then decreases. This shows that the influence of confining pressure on the test results is very significant. For the freezing-thawing soil samples, the damping ratio decreases by 20% during the loading test, and even exceeds 50% in some tests. The damping determines the amount of external energy absorbed by the soil. The greater the damping of the soil, the faster the attenuation of the vibration wave, and the more energy absorbed by the soil, which is converted into the deformation energy, the pore pressure, the kinetic energy and the friction heat energy. During the freezing process, the water molecules in the soil are frozen into ice crystals, and the pore volume expands. When the ice crystals melt and disappear, the pore volume in the soil becomes larger, and the soil has more deformation space. Under the cyclic loading, the soil is compressed and deformed and the energy absorbed by the soil increases, resulting in higher excess pore water pressure. However, the deformation increment is reduced due to the hardening of the soil. The area of the hysteresis loop is gradually reduced, and the damping of soil also decreased gradually.

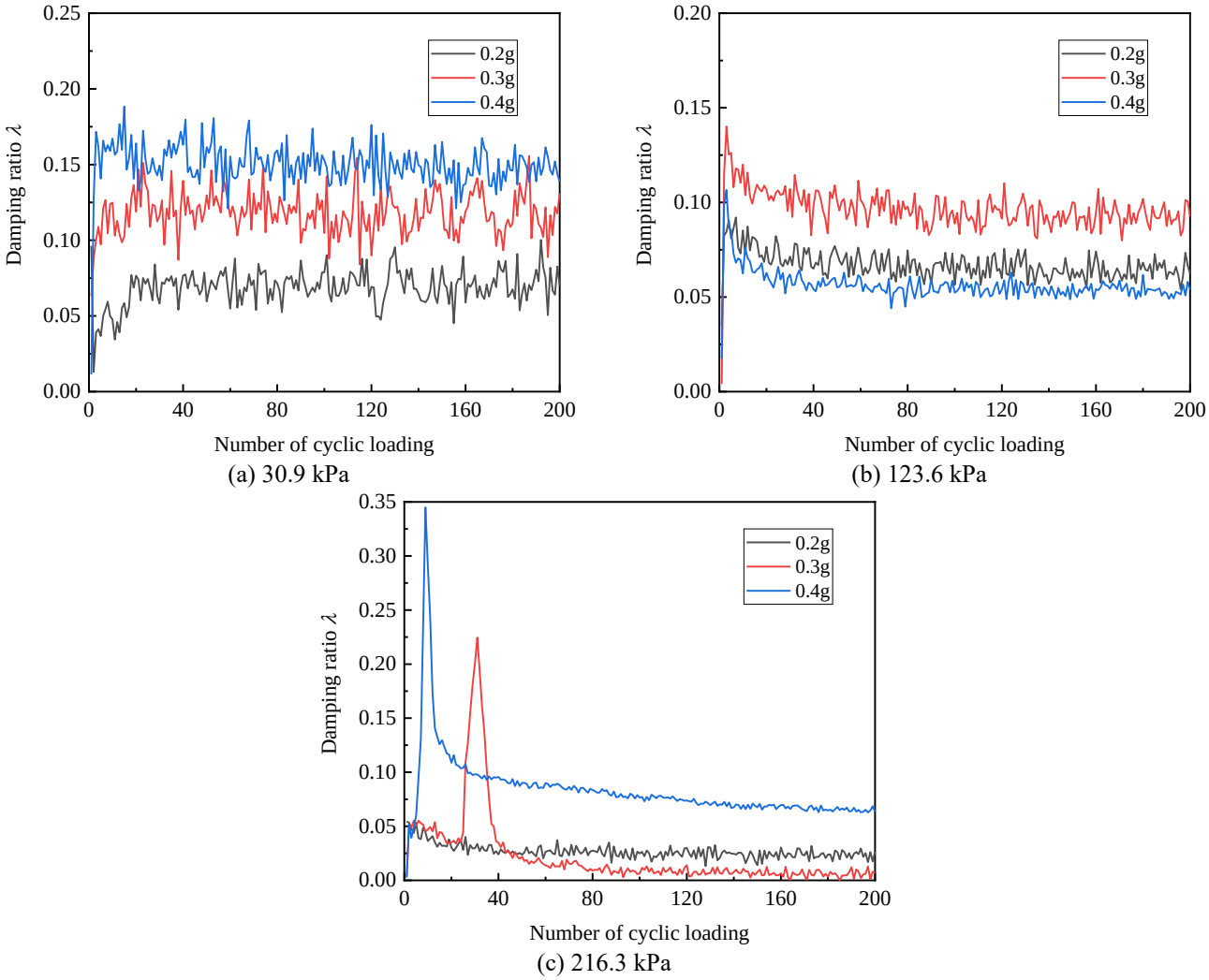

Fig. 11 Variations of the damping ratio with the number of cyclic loading for the freezing-thawing clay under the cyclic loading at different confining pressures: (a) 30.9 kPa, (b) 123.6 kPa and (c) 216.3 kPa

4. Conclusions

The cyclic triaxial tests were carried out to investigate the dynamic characteristics of freezing-thawing clay under the seismic loads. The reduction factor of dynamic shear stress is determined to correct the amplitude of seismic load. The deformation development mode, stress-strain relationship and energy dissipation behavior of freezing-thawing clay under the different confining pressures and dynamic stress amplitudes are evaluated and discussed. The main conclusions are as follows.

(1) When the confining pressure is small, the freezing-thawing clay exhibits the tensile strain under the cyclic loading. With the confining pressure increasing, the strain gradually develops to the compressive strain. It is speculated that there is a critical depth between 3 m and 12 m below the ground. When the effective confining pressure is less than it of critical depth, the specimen shows the tensile strain. When the effective confining pressure is greater than it of the critical depth, the specimen shows the compressive strain. The greater the peak ground acceleration, the faster the accumulative plastic strain of freezing-thawing clay develops.

(2) Based on the experimental data, an accumulative plastic strain model of freezing-thawing clay considering the confining pressure, the peak ground acceleration and the number of cyclic loading is proposed. The verification process shows that this model can be used to predict and calculate the accumulative plastic strain of freezing-thawing clay.

(3) The change of pore volume caused by freezing phase transition of pore water during freezing and thawing has a great impact on soil structures. Under the different confining pressures and dynamic stress amplitudes, the secant modulus of freezing-thawing clay shows a downward trend, indicating that the stiffness of soil weakens. Under the cyclic loading, the energy dissipation behavior and damping ratio of freezing-thawing clay gradually stabilizes.

Acknowledgements

This work presented in this paper was funded by the Graduate Innovation Program of China University of Mining and Technology (2022WLJCRCZL038) and the Postgraduate Research & Practice Innovation Program of Jiangsu Province (KYCX22_2574).

References

Afshani, A. and Akagi, H. (2015), "Artificial ground freezing application in shield tunneling", Japanese Geotech.Society Special Publication, **3**(2), 71-75. https://doi.org/10.3208/jgssp.v03.j01.

Alkire, B.D. and Morrison, J.M. (1983), "Change in soil structure due to freeze-thaw and repeated loading", *Transport. Res. Record*, **918**, 15-21.

Chamberlain, E.J. and Gow, A.J. (1979), "Effect of freezing and thawing on the permeability and structure of soils", *Eng. Geol*., **13**, 73-92. https://doi.org/10.1016/0013-7952(79)90022-X.

Cheng, S., Wang, Q., Fu, H., Wang, J., Han, Y., Shen, J. and Lin, S. (2021), "Effect of freeze-thaw cycles on the mechanical properties and constitutive model of saline soil", *Geomech. Eng*., **27**(4), 309-322. https://doi.org/10.12989/gae.2021.27.4.309.

Cui, Z.D., He, P.P. and Yang, W.H. (2014), "Mechanical properties of a silty clay subjected to freezing-thawing", *Cold Reg. Sci. Technol*., **98**, 26-34. https://doi.org/10.1016/j.coldregions.2013.10.009.

Cui, Z.D. and Zhang, Z.L. (2015), "Comparison of dynamic characteristics of the silty clay before and after freezing and thawing under the subway vibration loading", *Cold Reg. Sci. Technol*., **119**, 29-36. https://doi.org/10.1016/j.coldregions.2015.07.004.

Cui, Z.D., Zhang, Z.L., Yuan, L., Zhan, Z.X. and Zhang, W.K. (2019), "Design of underground structures", Springer Press, Singapore. https://doi.org/10.1007/978-981-13-7732-7.

Cui, Z.D., Zhang, L.J. and Zhan, Z.X. (2023), "Dynamic shear modulus and damping ratio of saturated soft clay under the seismic loading", *Geomech. Eng*., **32**(4), 411-426. https://doi.org/10.12989/gae.2023.32.4.411.

Ghazavi, M. and Roustaei, M. (2013), "Freeze-thaw performance of clayey soil reinforced with geotextile layer", *Cold Reg. Sci. Technol*., **89**, 22-29. https://doi.org/10.1016/j.coldregions.2013.01.002.

Guo, L., Liu, L.G., Wang, J., Jin, H.X. and Fang, Y. (2020), "Long term cyclic behavior of saturated soft clay under different drainage conditions", *Soil Dyn. Earthq. Eng*., 139. https://doi.org/10.1016/j.soildyn.2020.106362.

Iida, H., Hiroto, T., Yoshida, N. and Iwafuji, M. (1996), "Damage to Daikai subway station", *Soils Found*., **36**, 283-300. https://doi.org/10.3208/sandf.36.Special_283.

Jin, H., Go, G.-H., Ryu, B.H. and Lee, J. (2021), "Experimental and numerical investigation of closure time during artificial ground freezing with vertical flow", *Geomech. Eng*., **27**(5), 433-445. https://doi.org/10.12989/gae.2021.27.5.433.

Kang, M. and Lee, J.S. (2015), "Evaluation of the freezing-thawing effect in sand-silt mixtures using elastic waves and electrical resistivity", *Cold Reg. Sci. Technol*., **113**, 1-11. https://doi.org/10.1016/j.coldregions.2015.02.004.

Lei, H.Y., Song, Y.J., Qi, Z.Y., Liu, J.J. and Liu, X. (2019), "Accumulative plastic strain behaviors and microscopic structural characters of artificially freeze-thaw soft clay under dynamic cyclic loading", *Cold Reg. Sci. Technol*., 168. https://doi.org/10.1016/j.cohiregions.2019.102895.

Li, Q.L., Ling, X.Z., Wang, L.N., Zhang, F., Wang, J.H. and Xu, P.J. (2013), "Accumulative strain of clays in cold region under long-term low-level repeated cyclic loading: Experimental evidence and accumulation model", *Cold Reg. Sci. Technol*., **94**, 45-52. https://doi.org/10.1016/j.coldregions.2013.06.008.

Lin, B., Zhang, F., Feng, D.C., Tang, K.W. and Feng, X. (2017), "Accumulative plastic strain of thawed saturated clay under long-term cyclic loading", *Eng. Geol*., **231**, 230-237. https://doi.org/10.1016/j.enggeo.2017.09.028.

Ling, X.Z., Li, Q.L., Wang, L.A., Zhang, F., An, L.S. and Xu, P.J. (2013), "Stiffness and damping radio evolution of frozen clays under long-term low-level repeated cyclic loading: Experimental evidence and evolution model", *Cold Reg. Sci. Technol*., **86**, 45-54. https://doi.org/10.1016/j.coldregions.2012.11.002.

Ling, X.Z., Zhu, Z.Y., Zhang, F., Chen, S.J., Wang, L.N., Gao, X. and Lu, Q.R. (2009), "Dynamic elastic modulus for frozen soil from the embankment on Beiluhe Basin along the Qinghai-Tibet Railway", *Cold Reg. Sci. Technol*., **57**(1), 7-12. https://doi.org/10.1016/j.coldregions.2009.01.004.

Mansour, M.F. (2018), "Constitutive behavior of Port-Said Clay under seismic and small strain static conditions", *Ain Shams Eng. J.*, **9**(4), 2983-2991. https://doi.org/10.1016/j.asej.2018.06.005.

Murcia-Delso, J., Alcocer, S.M., Arnau, O., Martinez, Y. and Muria-Vila, D. (2020), "Seismic rehabilitation of concrete buildings after the 1985 and 2017 earthquakes in Mexico City", *Earthq. Spectra*, **36**(2), 175-198. https://doi.org/10.1177/8755293020957372.

Niemunis, A., Wichtmann, T. and Triantafyllidis, T. (2005), "A high-cycle accumulation model for sand", *Comput. Geotech*., **32**(4), 245-263. https://doi.org/10.1016/j.compgeo.2005.03.002.

Puppala, A.J., Saride, S. and Chomtid, S. (2009), "Experimental and modeling studies of permanent strains of subgrade soils", *J. Geotech. Geoenviron. Eng*., **135**, 1379-1389. https://doi.org/10.1061/(ASCE)GT.1943-5606.0000163.

Simonsen, E., Vincent C. Janoo, M.A. and Isacsson, U. (2002), "Resilient properties of unbound road materials during seasonal frost conditions", *J. Cold Reg. Eng*., **16**, 28-50. https://doi.org/10.1061/(ASCE)0887-381X(2002)16:1(28).

Singh, P., Bhartiya, P., Chakraborty, T. and Basu, D. (2023), "Numerical investigation and estimation of active earth thrust on gravity retaining walls under seismic excitation", *Soil Dyn. Earthq. Eng*., **167**, 107798. https://doi.org/10.1016/j.soildyn.2023.107798.

Tang, Y.Q. and Yan, J.J. (2015), "Effect of freeze–thaw on hydraulic conductivity and microstructure of soft soil in Shanghai area", *Environ. Earth Sci*., **73**(11), 7679-7690. https://doi.org/10.1007/s12665-014-3934-x.

Wang, D., Liu, E.L., Zhang, D., Yue, P., Wang, P., Kang, J. and Yu, Q.H. (2021), "An elasto-plastic constitutive model for frozen soil subjected to cyclic loading", *Cold Reg. Sci. Technol*., **189**, 103341. https://doi.org/10.1016/j.coldregions.2021.103341.

Wang, D.Y., Ma, W., Niu, Y.H., Chang, X.X. and Wen, Z. (2007), "Effects of cyclic freezing and thawing on mechanical properties of Qinghai-Tibet clay", *Cold Reg. Sci. Technol*., **48**(1), 34-43. https://doi.org/10.1016/j.coldregions.2006.09.008.

Wang, S., Wang, Q., Xu, J., Ding, J., Qi, J., Yang, Y. and Liu, F. (2019), "Thaw consolidation behavior of frozen soft clay with calcium chloride", *Geomech. Eng*., **18**(2), 189-203. https://doi.org/10.12989/gae.2019.18.2.189.

Wang, Z.Z., Gao, B., Jiang, Y.J. and Yuan, S. (2009), "Investigation and assessment on mountain tunnels and geotechnical damage after the Wenchuan earthquake", Science in China Series E-Technological Sciences, **52**(2), 546-558. https://doi.org/10.1007/s11431-009-0054-z.

Wichtmann, T., Rondón, H.A., Niemunis, A., Triantafyllidis, T. and Lizcano, A. (2010), "Prediction of permanent deformations in pavements using a high-cycle accumulation model", *J. Geotech. Geoenviron. Eng*., **136**, 728-740. https://doi.org/10.1061/(ASCE)GT.1943-5606.0000275.

Yang, Y.G., Lai, Y.M. and Li, J.B. (2010), "Laboratory investigation on the strength characteristic of frozen sand considering effect of confining pressure", *Cold Reg. Sci. Technol*., **60**(3), 245-250. https://doi.org/10.1016/j.coldregions.2009.11.003.

Yao, X.L., Qi, J.L. and Ma, W. (2009), "Influence of freeze-thaw

on the stored free energy in soils", Cold Regions Sci. Technology, **56**(2-3), 115-119. https://doi.org/10.1016/j.coldregions.2008.11.001.

Yilmaz, F. and Fidan, D. (2018), "Influence of freeze-thaw on strength of clayey soil stabilized with lime and perlite", *Geomech. Eng.*, **14**(3), 301-306. https://doi.org/10.12989/gae.2018.14.3.301.

Zhang, Z.L. and Cui, Z.D. (2018), "Effect of freezing-thawing on dynamic characteristics of the silty clay under K0-consolidated condition", *Cold Reg. Sci. Technol.*, **146**, 32-42. https://doi.org/10.1016/j.coldregions.2017.11.009.

Zheng, L.F., Gao, Y.T., Zhou, Y., Liu, T. and Tian, S.G. (2021), "A practical method for predicting ground surface deformation induced by the artificial ground freezing method", *Comput. Geotech.*, 130. https://doi.org/10.1016/j.compgeo.2020.103925.

Zhou, J. and Tang, Y.Q. (2015a), "Artificial ground freezing of fully saturated mucky clay: Thawing problem by centrifuge modeling", *Cold Reg. Sci. Technol.*, **117**, 1-11.https://doi.org/10.1016/j.coldregions.2015.04.005.

Zhou, J. and Tang, Y.Q. (2015b), "Centrifuge experimental study of thaw settlement characteristics of mucky clay after artificial ground freezing", *Eng. Geol.*, **190**, 98-108. https://doi.org/10.1016/j.enggeo.2015.03.002.

Zhou, Z.W., Ma, W., Zhang, S.J., Mu, Y.H. and Li, G.Y. (2018), "Effect of freeze-thaw cycles in mechanical behaviors of frozen loess", *Cold Reg. Sci. Technol.*, **146**, 9-18. https://doi.org/10.1016/j.coldregions.2017.11.011.

GC